J Mater Sci (2007) 42:5046–5056
DOI 10.1007/s10853-006-0579-5

Microstructural characterization and fracture properties of SiC-based fibers annealed at elevated temperatures

J. J. Sha · T. Hinoki · A. Kohyama

Received: 6 April 2006 / Accepted: 15 June 2006 / Published online: 22 February 2007

Abstract Ceramic matrix composites (CMCs) have been proposed as potential structural materials for application of high temperature technologies. Excellent high temperature performance of CMCs requires that fibers must have high enough thermal stability and sufficient mechanical properties throughout the service life. In order to clarify the correlation between the mechanical properties and the microstructure of SiC-based fibers, SiC-based fibers were annealed at elevated temperatures in Ar for 1 h. After annealing, the fracture strengths on these fibers were evaluated at room temperature by tensile test; the microstructural features were characterized by X-ray diffraction (XRD) and field emission scanning electron microscopy (FE-SEM). Furthermore, the fracture mechanics was applied to estimate the fracture toughness and the critical fracture energy of these fibers. As a result, excellent microstructure and mechanical stabilities were observed for SiC fibers with near-stoichiometric composition and high-crystallite structure. Combining the microstructure examination with tensile test indicates that the thermal and mechanical stabilities of SiC fibers at high temperatures were mainly controlled by their crystallization and composition as well as other factors.

J. J. Sha (✉)
International Innovation Center, Kyoto University,
Sakyo-ku, Kyoto 606-8501, Japan
e-mail: shajianjun@iic.kyoto-u.ac.jp

T. Hinoki · A. Kohyama
Institute of Advanced Energy, Kyoto University, Gokasho,
Uji, Kyoto 611-0011, Japan

Introduction

Currently, ceramic matrix composites (CMCs) have been proposed as potential structural materials for application of high temperature technologies, such as advanced energy-generation systems and propulsion systems [1–3]. The key to successful application of CMCs is judicious selection and incorporation of ceramic fiber reinforcement with proper chemical, physical and mechanical properties. For high temperature operation, the most critical fiber properties are high strength and its reliable retention throughout the service life. Low fiber strength and thermal stability could result in low fracture toughness and accelerate sub-critical crack propagation in CMCs.

Recently developed SiC-based fibers with near-stoichiometric composition and high-crystallite structure, such as Hi-Nicalon^{TM} type S [4] and Tyranno^{TM}-SA [5], are promising reinforcement for CMCs fabrication. These fibers experienced a pyrolysis or sintering process during fabrication and their microstructure and mechanical properties depend on the thermal history. On the other hand, CMCs may be applied or fabricated above the fiber's processing temperature [1–3, 6, 7]. In many cases, SiC fibers were expected to expose to an environment with very high temperature and low oxygen partial pressure in which case, the performance of fibers could be changed by thermal exposure, since the thermal and mechanical stability of SiC fibers, which can vary with processing conditions, are very sensitive to high temperature environment.

The processing, structure and composition on as-received SiC fibers have been presented in literature [8]. These authors confirmed the chemical composition

of SiC fibers with several techniques, and revealed some other original features: The carbon-rich layer on the surface of the HNLS fiber (80 nm) is much thicker than that of HNL fiber (20 um); Tyranno-SA fiber (about 10 um in diameter) has a carbon-rich core indicating that near-stoichiometric composition is only effective near edge region. Similar phenomenon on Tyranno-SA fiber was also observed by Colomban et al. using the Raman Spectroscopy [9, 10]. Bunsell et al. [11] also reported that both Hi-Nicalon Type S and Tyranno-SA fiber contain excess carbon at triple points of grain boundaries. The microstructure of SiC materials in high temperature and oxidative environment is very sensitive to composition. Consequently, it is necessary to characterize the microstructure of SiC fibers at elevated temperatures in order to know the degradation mechanism and to predict high temperature performance of CMCs.

In our former work [12], the tensile properties of the annealed SiC fibers were investigated by tensile test, and fundamental analysis on the microstructure of these fibers was performed by means of field-emission scanning electron microscopy (FE-SEM) and X-ray diffraction (XRD), but no attempts were made to correlate the microstructure and the fracture properties. As observed in this work [12], the fracture of the Hi-Nicalon^{TM} and the Hi-Nicalon^{TM} Type S fibers mainly originated from critical flaw and showed a clear fracture mirror zone. Therefore, for practical application of CMCs, it is requested to accumulate experimental data and to reveal the degradation mechanism of SiC fibers with a consideration of the thermal-chemical stability.

In order to identify the factors, which affect the high temperature performance of SiC fibers, this work proceeded a complementary investigation on the microstructure features and fracture properties of SiC fibers annealed at elevated temperatures, and attempted to clarify the correlation between the mechanical properties and the microstructure. The fracture toughness and the critical fracture energy at elevated temperatures were estimated using the fracture mechanics by measurement of the critical flaw size/mirror size.

Experimental procedure

Materials and annealing condition

The fibers examined in this study were Hi-Nicalon^{TM} (HNL: C/Si = 1.39, oxygen = 0.5 wt%, diameter: 14 um), Hi-Nicalon^{TM} Type-S (HNLS: C/Si = 1.05, oxygen = 0.2 wt%, diameter: 12 um) and Tyranno^{TM} SA (TySA (Grade 3): C/Si = 1.05, oxygen < 0.5 wt%, alumina < 1 wt%, diameter: 7 um). It is clear that HNL fiber contained excess carbon and low oxygen content. The latter two have near-stoichiometric composition and high crystallinity. These fibers were put in a graphite crucible and then annealed in Ar under a pressure of 10^5 Pa and held for 1 h at desired temperature from 1,300 to 1,900 °C. The annealing condition has been described in more detail elsewhere [12].

Characterization

After annealing, several techniques were used to characterize the fiber microstructure features and fracture properties. The XRD with CuKα irradiation was applied to examine the present phase, and the apparent crystallite size of β-SiC was estimated by employing the Scherrer formula [13]:

$$L = K \cdot \lambda / (D \cdot \cos\theta) \quad (1)$$

where K is a constant (taken as 0.9), λ the CuKα wavelength (i.e., $\lambda = 0.154056$ nm), D the half-value width of β-SiC (111) peak and θ the Bragg angle ($\theta = 17.5°$ for β-SiC (111)).

FE-SEM image analyses were carried out within a fiber tow and along the fiber length to check the diameter variation. Result showed that these fibers had a wide diameter variation within a tow. The diameter variations within a tow are 10.78–16.60 um for the HNL fiber, 10.85–14.04 um for the HNLS fiber, 5.20–9.67 um for the TySA fiber, respectively. Based on this result, the individual fiber diameter was measured for precise strength calculation. FE-SEM was also used to characterize the fiber's surface morphologies and fracture surface.

Furthermore, the critical flaw size and fracture mirror size on the fracture surfaces of fiber fragments were measured by means of FE-SEM examination. The fracture fragments were obtained by single filament tensile tests, which were performed at room temperature in ambient atmosphere using a mechanical testing apparatus (Instron Corp. Model 5581) according to ASTM-recommended procedures [14]. The load was applied at a constant strain rate of 2×10^{-4}/s and measured by a load-cell of 2.5 N. The individual filaments had a gauge length of 25.4 mm and were aligned and glued on cardboard fixture with epoxy. For each fiber type, the total number of tests is ≥20. The detailed testing procedure has been presented in the literatures [12, 15].

Results and discussion

XRD characterization

Figure 1a–c showed X-ray diffraction patterns of three types of fibers annealed at elevated temperatures in Ar for 1 h. The XRD patterns of the as-received SiC fibers show three main peaks which were assigned to the (111) ($2\theta = 35.7°$; $d = 0.251$ nm), (220) ($2\theta = 60.0°$; $d = 0.154$ nm) and (311) ($2\theta = 72.0°$; $d = 0.131$ nm). The phases present in the HNL fibers were β-SiC and XRD-amorphous carbon. After annealing at temperature over 1,400 °C, two other peaks are also observed and peak height increased with increasing the annealing temperature, which are indexed as the (200) and (222) crystal planes and more obvious in HNLS fibers annealed at temperatures over 1,600 °C (Fig. 1b).

The diffraction peaks in HNL fiber become sharp and narrow when temperature is higher than 1,300 °C (Fig. 1a), while they are not so obvious for near-stoichiometeric fibers (Fig. 1b, c). Such changes in the diffraction peaks of HNL fibers are due to the coalescence of β-SiC nano-crystals caused by the decomposition of the intergranular amorphous phase and thermally activated diffusion. The decomposition of the intergranular amorphous SiC_xO_y phase occurred at about 1,300 °C in HNL fiber resulted in progressive crystallization of β-SiC according to the reaction [16]:

$$SiC_xO_y \rightarrow SiC(s) + SiO(g) + CO(g) \quad (2)$$

The very sharp diffraction peaks of β-SiC in as-received HNLS and TySA fibers indicated that these fibers have already been high-crystallite structure (Fig. 1b, c), because of their very high fabrication temperature (about 1,600 °C and 1,800 °C for HNLS and TySA, respectively). The annealing at temperatures beyond 1,600 °C caused gradual crystallization of β-SiC in HNLS fiber (Fig. 1b).

Using the Scherrer's formula, the apparent crystallite size of β-SiC, D_{SiC}, was calculated from the half-value width of the (111) peak. The plot of the β-SiC crystallite size as a function of annealing temperature was shown in Fig. 2. Following features were observed: (i) The grain coarsening of HNL fiber started at 1,400 °C. (ii) the crystallite size of β-SiC in HNLS and TySA fiber remained almost constant as annealing temperature < 1,600 °C, while higher temperature annealing caused an continuous coarsening in crystallite size of SiC in HNLS. The crystallite size of β-SiC in TySA fibers appears to be little dependent on the annealing temperature. The crystallite sizes for as-received HNL, HNLS and TySA fibers are 4.0, 11.4, and 22.7 nm, while they are 15.5, 30.3, and 25.5 nm for fibers annealed at 1,900 °C for 1 h, respectively.

The grain coarsening could be attributed to the coalescence of β-SiC nanocrystals due to either decomposition of amorphous phase or diffusion of Si and C atoms at grain boundaries during exposure at high temperatures. For the bulk materials with clean grain boundaries, the grain growth proceeds through

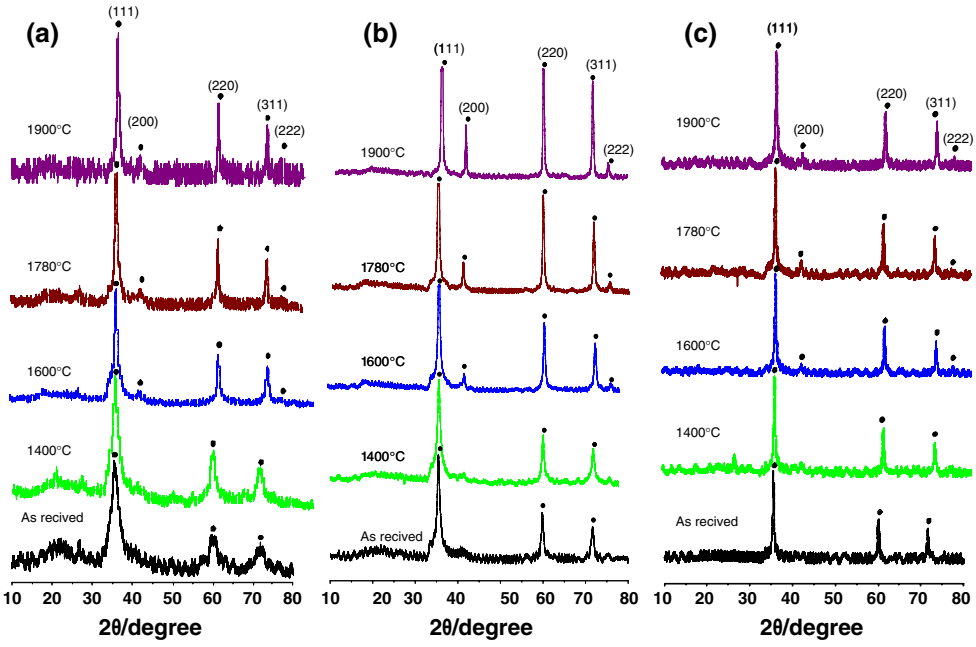

Fig. 1 X-ray diffraction patterns for SiC fibers annealed at elevated temperatures: (**a**) HNL fiber; (**b**) HNLS fiber; (**c**) TySA fiber : β-SiC

large grains incorporating the small one by grain boundary diffusion. Especially, for grains with small size, the grain boundary diffusion operates much more readily. As observed in two Nippon Carbon fibers, the grain coarsening is more obvious in annealed state than those of as-received state (TEM observations have revealed that grain size is about 5 nm for HNL fiber [17], 20 nm for HNLS fiber [18], 200 nm for TySA fiber [11]). On the other hand, the residual trace oxygen may play a role in the Si and C grain boundary transport by accelerating diffusion [17], because the oxygen is not necessarily eliminated from the fiber as reported in the literature [8], even for the HNLS fiber which was fabricated at very high temperature.

Considering the starting temperature for grain coarsening in Fig. 2, the grain size might be related primarily to the maximum temperature at which the fibers were fabricated. The fabrication temperatures have been presented for two Nippon Carbon fibers (HNL: 1,350 °C, HNLS: 1,600 °C) and for TySA fiber (about 1,800 °C) in the literature [19]. From the Fig. 2, it can be seen that the crystallite size increased when annealing temperature is above the fabrication temperature as expected. For HNL fiber, the grain coarsening occurred at relatively low temperature is due to the decomposition of amorphous phase at about 1,300 °C. On the other hand, the thermally activated diffusion plays an important role on the grain coarsening of SiC materials at high temperatures.

If we make a further comparison in crystallite size between two Nippon Carbon fibers again, we can see that a large difference in crystallite size was observed for two fibers annealed at same temperature. As above mentioned, the HNL fiber has an small starting grain size, which was expected to have a high diffusivity at grain boundaries and result in a large grain size as annealing at high temperatures. However, an unexpected phenomenon was observed between two Nippon Carbon fibers. This can be attributed to the excess carbon in HNL fiber. TEM observation revealed that heat treatment of the HNL fiber results in a gradual organization of the free carbon phase in terms of the size of the carbon layer and the number of stacked layers as increasing temperatures [17]. Takeda et al. [20] have investigated the properties of polycarbosilen-derived silicon carbide fibers with various C/Si compositions, and revealed that microstructure and mechanical properties are quite dependent on the C/Si composition. Grain growth is suppressed with increase in excess carbon. In other studies [21, 22], the carbon suppressing growth and coalescence of the SiC microcrystals was also observed. Sasaki [22] found that carbon disappeared above 1,500 °C heat treatment in SiC fiber using Raman study. And then an abrupt increase of crystal size at 1,500 °C was observed.

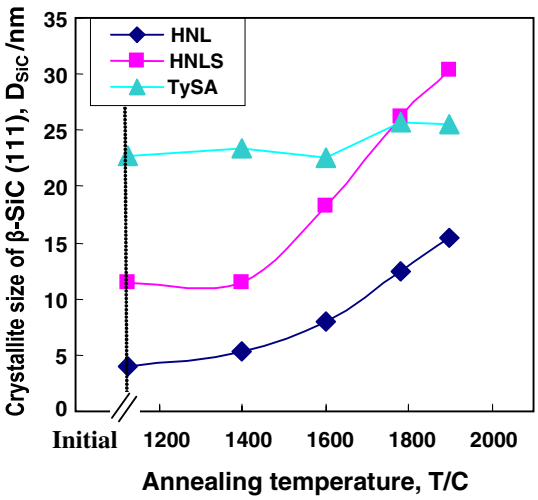

Fig. 2 Apparent crystallite size of β-SiC for SiC fibers annealed at elevated temperatures in Ar for 1 h

For the TySA fiber, this fiber originally has a very large crystallite size. In previous studies [8–10], a carbon-rich core was revealed in TySA fiber, which results from the production process. Colomban et al. estimated carbon grain size and SiC grain size in TySA fiber from Raman spectroscopy [9, 10]. The Carbon grains appear approximately 2–3 times smaller on the fiber's core (0.9–1.7 nm) than on its periphery (1.7–2.6 nm). The grain size of SiC in fiber core is much smaller than edge region. Likely, this is due to that carbon suppressed the grain growth of β-SiC. Furthermore, this fiber contains the small amount of alumina (less than 1 wt%) as sintering additive, which will also inhibit the grain growth of SiC. As a result, the TySA fiber showed an excellent thermal stability in Ar atmosphere.

Tensile strength

Tensile strengths were obtained by a single filament tensile test technique at room temperature. If plotting the tensile data into the Fig. 2, it is obvious that the strengths of annealed fiber were related to β-SiC crystallite size (D_{SiC}) as shown in Fig. 3. The Fig. 3 confirmed the fact that generally materials with large grain size have low strengths. The growth of SiC crystals reduces the bonding forces at the grain boundaries. Since the manufactures are always seeking the optimal fabrication temperature at which the superior thermal stability and excellent mechanical strength can be obtained simultaneously, thus, the upper fabrication temperatures are typically fixed by

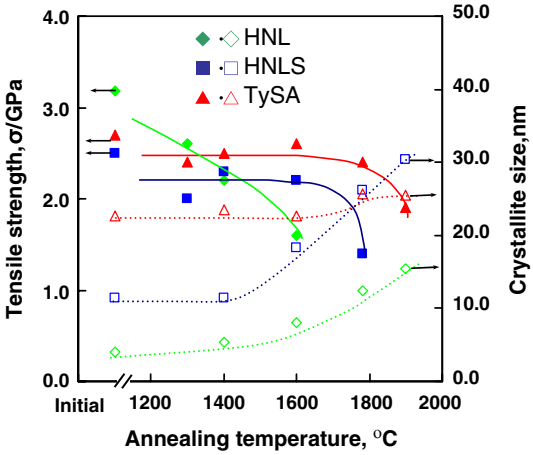

Fig. 3 Tensile strength and its relation to the crystallite size for SiC fibers annealed at elevated temperatures in Ar for 1 h

those temperature conditions above which performance degradation of the fibers occurred. The dependence of strength on temperature in present study is in agreement with those of previous studies [5, 17, 18, 22]. Ichikawa et al. [18] reported that HNLS was quite stable chemically after 1 h exposure in an argon gas at 1,800 °C, since no structural decomposition occurred and it exhibited a good strength of 1.9 GPa. The crystallite size is about 35 nm. TEM observation shows that this annealed HNLS fiber has a SiC grain size of approximately 200 nm, which is about 10 times larger than that of the as-received fiber.

As for TySA fiber, this is a sintering fiber, which is prepared by the reaction of a polycarbosilane (PCS) with aluminiumacetylacetonate, and subsequently converted into the Tyranno SA fiber, by decomposition with an evolution of CO and SiO (1,500 °C $< T <$ 1,700 °C) and sintering (about 1,800 °C). TySA fiber retained most of its initial strength, because no significant grain coarsening was observed even annealed at 1,900 °C. Excellent strength retention has been observed in a former work [5].

On the other hand, the HNL fiber has smaller crystal size comparing to that of HNLS fiber, but it showed more rapid strength degradation than HNLS fiber above 1,400 °C annealing as shown in Fig. 3; both HNLS and TySA fiber have near-stoichiometric composition and high-crystallite structure, but they showed different strength retention. This observed phenomenon implied that other mechanisms must be responsible for strength degradation of SiC fibers besides the coarsening of crystallite size.

One source for strength degradation is residual stresses, which were generated from phase transformation and the mismatch in the coefficient of thermal expansion between excess carbon and SiC grain. Sacks [23] produced a laboratory fiber (UF fiber) with the similar composition as HNL fiber. There was no loss in strength with heat treatments up to 1,700 °C and then the strength decreased rapidly with further heat treatments up to 1,900 °C. He believed that strength is controlled by the residual tensile stresses, which developed as a result of the mismatch in thermal expansion coefficient between SiC and C. This situation should be true. The coefficient of thermal expansion of carbon/graphite ($2.0–3.0 \times 10^{-6}$/K) is less than SiC ($3.9–4.0 \times 10^{-6}$/K). When fibers were cooled from high annealing temperature to room temperature, the SiC grains want to contract, while carbon grain will resist their contraction. This action-reaction will put SiC in tension and carbon in compression. This residual tension stresses could have a contribution to the total stress loss. This case can be applied to each fiber type, which contains excess carbon, but here it should be more significant in HNL fiber because of high excess carbon (C/Si = 1.38). In both HNL fiber and TySA fiber, the size of carbon grain increased with increasing annealing temperature [9, 10, 17]. The growth of the carbon corresponds to a decrease of localized spin centres [24]. The growth of the carbon grain might result in an increase of residual stress however, this evidence is insufficient because the magnitude of residual stresses is strongly dependent on the volume fraction of carbon phase in a bulk material.

Surface morphologies

Figure 4 showed SEM morphologies of the fibers after annealing at elevated temperatures in Ar for 1 h.

The HNL fibers annealed at temperatures below 1,400 °C had a smooth surface, which is almost no difference from that of as received fibers (Fig. 4a). Annealing at 1,400 °C caused slight coarsening of fiber surface (Fig. 4b). Obvious changes in appearance were observed for the fibers annealed at 1,780 °C. These fibers showed a porous microstructure and large grains deposition on the fiber surface (Fig. 4c). Such huge crystals are not observed within bulk of the fiber, due to the presence of free carbon, which inhibit the grain boundary or/and gaseous diffusion.

For the HNLS fibers annealed below 1,600 °C, their microstructure did not vary compared to the as-received fibers (Fig. 4d). After annealing at 1,600 °C, although the individual SiC grain grown on the fiber surface, but fiber surface still remained smooth and it appeared no structure degradation (Fig. 4e). The fiber annealed at 1,780 °C exhibited a rough surface with deposition of bulk SiC grains, but it still remained a relatively dense structure (Fig. 4f).

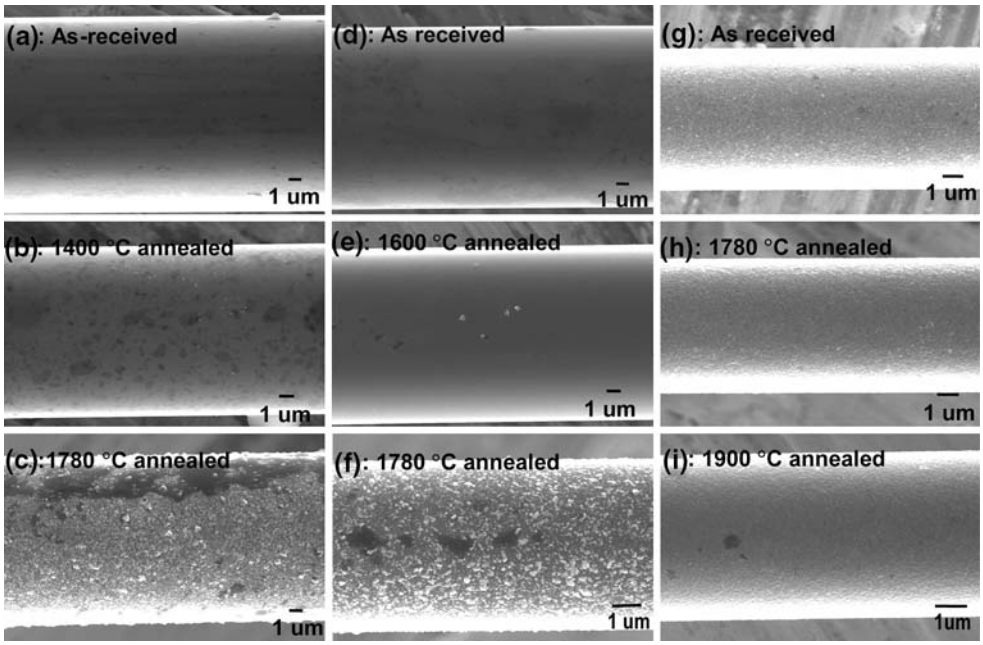

Fig. 4 SEM photographs for SiC fibers annealed at elevated temperatures in Ar for 1 h: (**a–c**) HNL fibers; (**d–f**) HNLS fibers; (**g–i**) TySA fibers

TySA fibers showed outstanding thermal stability in microstructure comparing with other SiC fibers and didn't exhibit obvious structure damage in all annealing conditions (Fig. 4g–i).

The formation of porous structure in HNL fiber could be attributed to the rapid evolution of gases at the earlier stage of high-temperature exposure according reaction (2). It should be noted that large grains grown outward from the surface of fibers at 1,780 °C appear to be β-SiC crystals, which were produced by following gas-phase reactions [25, 26].

$$SiO(g) + 3CO(g) \rightarrow SiC(s) + 2CO_2(g) \quad (3)$$

$$SiO(g) + 2C(s) \rightarrow SiC(s) + CO(g) \quad (4)$$

Reaction (4) could occur because of presence of free carbon in surface and body of HNL fibers [27]. According to above result, the reaction (2)–(4) are quite dependent on the quantity of amorphous phase and content of carbon in SiC fibers. The use of graphite crucible could cause the reaction:

$$CO_2(g) + 2C(s) \rightarrow 2CO(g) \quad (5)$$

Combing the reaction (3) and (5) indicating the gas-phase reaction proceeded mainly by reaction (4). Additionally, the CO–CO_2 gas mixture might modify the microstructure of SiC fibers at high temperatures [28].

Considering the surface degradation of HNLS fibers annealed above 1,600 °C (Fig. 4f), as we know, the quantity of amorphous phase and oxygen content should be very small in this fiber. Thus, thermal decomposition of the amorphous phase is almost negligible in this fiber. As for the large grains deposited on the surface of HNLS fiber, it can be explained by reactions (3)–(5), because the carbon layer on the surface of HNLS fiber (80 nm) is thicker than that of HNL fiber (20 nm) [8]. Concerning the origin of gas species, other mechanism could be responsible for this. Active oxidation is quite possible in this study.

In this work, the oxygen partial pressure in furnace chamber was calculated to be 2×10^{-1} Pa (based on the oxygen concentration in Ar (2 ppm) and total pressure (10^5 Pa)). The transition from passive oxidation to active oxidation occurs at oxygen partial pressure of 10–25 Pa and 1–2.5 Pa at 1,500 °C for HNL and HNLS fiber [26], respectively. Additionally, the value of oxygen partial pressure for passive-to-active transition increased with increasing the exposure temperature [25]. Therefore, at same oxygen partial pressure level, the increased heat treatment temperature will accelerate the transition from passive-to-active oxidation. The active oxidation of SiC at high temperature and low oxygen partial pressure mainly proceeded by following reaction [25].

$$SiC(s) + 1/2O_2(g) \Leftrightarrow SiO(g) + C(s) \quad (6)$$

$$SiC(s) + O_2(g) \Leftrightarrow SiO(g) + CO(g) \quad (7)$$

Meanwhile, the thermal decomposition of the amorphous phase in HNL fiber, yields a porous fiber structure. Subsequent active oxidation is accelerated greatly, because of its high permeability to oxygen gas.

In addition, the specific grain boundary area in HNL fiber is much higher than those of other fibers because of its very fine grain size. The oxygen diffusion is very rapid in grain boundaries but very slow in the lattice. All these factors would lead to that the HNL fiber is more susceptible to active oxidation. The large grain deposited on the surfaces of Nippon carbon fibers can be formed by gas-phase reaction due to generation of gas species (SiO and CO) from active oxidation.

For the TySA fiber, the excellent microstructure stability could be attributed to the high processing temperature (over than 1,800 °C) and addition of alumina [5]. The small amount of alumina addition could inhibit the grain growth and enhanced the corrosion resistance. This higher stability can also be linked to the silica protective layer formed on the surface of fiber [9, 29].

Characterization of fracture surface

Obvious differences were observed in subsequent observations of fracture surface. The fracture of as-received HNL and HNLS fibers mainly originated from the inner critical flaw (inclusion-type or inner pore-type critical flaw). Linking these micrographs to the production process, the defects such as inclusion or bubbles from impurities or un-melted precursors may exist in polycarbosilane-derived fibers. These defects may generate local internal stress concentration during the process and subsequently lead to crack formation in tension. Under same processing parameters, it is likely that the stress concentration will vary with varying fiber diameter, since it is easier to relax the stress concentration in a fiber with fine diameter. After annealing at 1,600 °C, most of the examined HNL and HNLS fibers fractured at surface flaw as shown in Fig. 5a–f, and flaw size slightly increased with increasing annealing temperature. The critical flaw size and mirror size were measured based on the region definition in literatures [30, 31]. The critical flaw sizes (r_c) are: 0.90 μm for as received HNL fiber, 1.07 μm for 1,600 °C annealed HNL fiber. In case of HNLS fiber, the critical flaw sizes (r_c) are: 0.84 μm for as received fibers, 0.90 μm for 1,600 °C heat treated fibers.

Linking the tensile strength data in Fig. 3 with the microstructure examination (Fig. 4 and 5) again, the quick decomposition of amorphous phase, grain coarsening and active oxidation at high temperatures in HNL fiber could be responsible for strength and microstructure degradation. The active oxidation generated gas species and damaged the fiber's surface, as observed on the fracture surfaces that annealed HNL and HNLS fiber mainly fractured at surface defect. A surface defect is easily to initiate the crack because of the stress concentration under tension, resulting in the degraded strength. Above 1,600 °C, the outward growth of huge grains was observed, and these huge grains might act as the critical flaw during the fracture of fiber. Observation of surface morphologies (Fig. 4) and fracture surface (Fig. 5) provided a good evidence for the strength degradation of SiC fibers. Due to near-stoichiometric composition in HNLS fiber, its damage was limited on the surface of fiber.

Figure 5f showed that fracture surface of the TySA fibers after annealing at 1,900 °C did not reveal obvious difference in the fracture mode comparing with the as-received fibers. The fracture origin and mirror zone are invisible on the fracture surface and fracture surface showed a trans-crystallite fracture behavior. In order to see the fracture mode of this fiber clearly, the magnified SEM fractographs were shown in Fig. 6. It can also be seen from Fig. 6 that carbon seems distributed in grain boundaries, and the size in annealed fiber is somewhat larger than that of as-received one. Colomban et al. have also found that carbon-rich core existed in TySA fiber and carbon grain size increased after annealing at 1,600 °C by Raman spectroscopy [10]. The trans-crystallite fracture behavior could be partially related to a high compression residual stress in SiC caused by addition of alumina in this fiber. Existence of compression residual stresses in the grain boundary of TySA fiber is quite possible because of significant mismatch in the coefficient of thermal expansion between SiC and Alumina (SiC: 3.9–4.0×10^{-6}/K; Alumina: 8.0–9.0×10^{-6}/K) and high sintering temperature (higher than 1,800 °C). In TySA fibers, the change in the extension stability of microcrack in the compression residual stress filed might improve the grain boundary strength. The increase in grain boundary strength could explain the trans-crystalline fracture behavior of TySA fiber.

Fracture toughness and critical fracture energy

Fracture toughness

For the brittle ceramic materials, according to the Griffith theory, the fracture mechanics could be applied to estimate the fracture toughness of these SiC fibers [30–32]. Figure 7 shows the dependence of strength on critical flaw size for as-received HNL and HNLS fiber. From this plot, it can be seen that the strength decreased with an increase of critical flaw size, and the slops of fitting lines by linear regression analysis are approximate –0.5, indicating the fracture mechanics can be applied to present study. Similar result has also been observed in other SiC fibers [15, 30, 31].

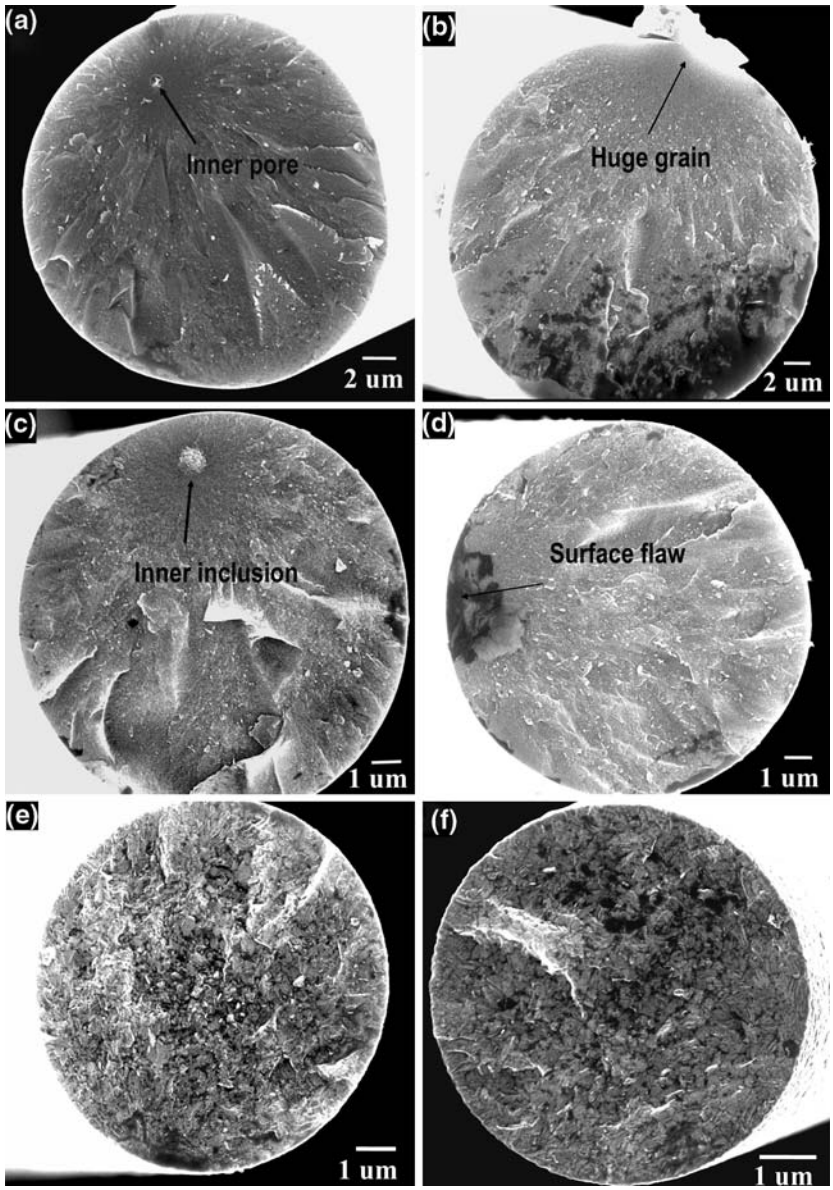

Fig. 5 Typical fracture surface observation in: (**a**) as-received HNL fiber; (**b**) 1,600 °C annealed HNL fiber;(**c**) as-received HNLS fiber; (**d**) 1,600 °C annealed HNLS fiber; (**e**) as-received TySA fiber; (**f**) 1,900 °C annealed TySA fiber

Fracture mechanics predicts a relation between flaw radius, fracture strength (σ_f) and fracture toughness (K_{1c}), where K_{1c} is the mode 1 fracture toughness of the SiC fiber.

$$\sigma_f(r_c)^{1/2} = YK_{1c} = \text{constant} \tag{8}$$

In Eq. (8), Y is a geometric factor dependent on the critical flaw shape and location and its relative size compared to the fiber dimension. Y is 1.56 for a small, centrally located penny-shaped flaw in a plane normal to the tensile axis given in the Ref. [32].

Additionally, it has been observed that the product of strength, σ_f, and the square root of mirror size obeyed following formula [30–33]

$$\sigma_f = A_m(r_m)^{-0.5} \tag{9}$$

where A_m is the mirror constant.

Substituting σ_f in Eq. (8) with Eq. (9), the fracture toughness, K_{1c}, could be expressed as:

$$K_{1c} = A_m(r_c/r_m)^{0.5}/Y \tag{10}$$

The ratio of critical flaw size (r_c) to mirror size (r_m) in present work was measured to be about 0.39. In Fig. 8, the tensile strength σ_f versus $(r_m)^{-0.5}$ are plotted for HNL and HNLS fiber, respectively. The data were fit to a line by linear regression analysis. The mirror constant A_m, defined as the slope of the fitting line in Fig. 8, was determined to be 3.93 $MPam^{1/2}$ for HNL fiber,

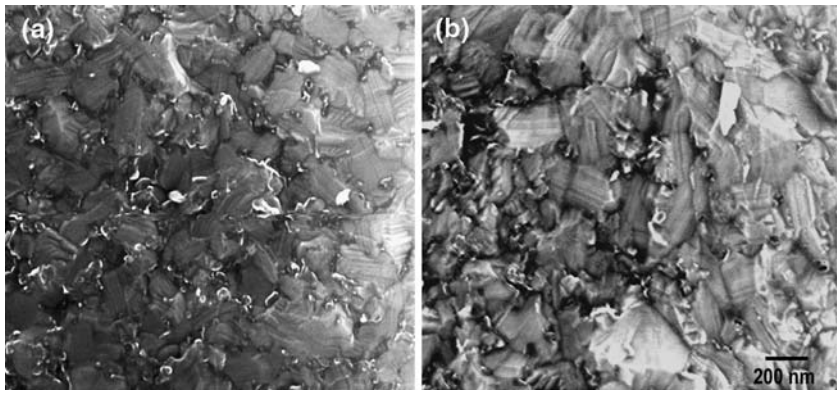

Fig. 6 Magnified SEM photographs on the fracture surface of TSA fiber: (**a**) as-received; (**b**) annealed at 1,900 °C

4.33 $MPam^{1/2}$ for HNLS fiber, respectively. From $K_{1c} = A_m(r_c/r_m)^{0.5}/Y$, using $r_c \approx 0.39\ r_m$ and $Y = 1.56$, the calculated K_{1c} is 1.56 $MPam^{1/2}$ for as-received HNL fiber, 1.74 $MPam^{1/2}$ for as-received HNLS fiber. Since A_m is an average value, the K_{1c} value determined for these fibers also is an average value. The K_{1c} for polycrystalline SiC is ≈ 2 MPa $m^{1/2}$, while that for most amorphous ceramics is ≈ 0.5 to 1 MPa $m^{1/2}$ [33]. For the annealed fibers, the resultant value of fracture toughness was listed in Table 1. The fracture toughness decreased with increasing the annealing temperature, but it did not show strong dependence on the annealing temperature.

Critical fracture energy

Attempts have been made to relate the critical flaw radius to the critical fracture energy, γ_c, which can be obtained from the following equations [30, 31],

$$r_c = Y^2 2E\ \gamma_c/\sigma_f^2 \tag{11}$$

$$\sigma_f \cdot r_c^{1/2} = Y\sqrt{2E\ \gamma_c} \tag{12}$$

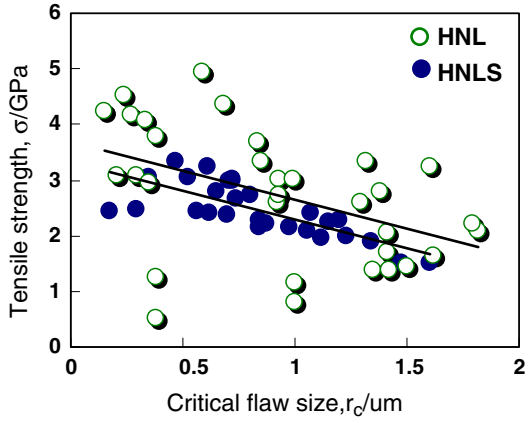

Fig. 7 The dependence of tensile strength on critical flaw size in as-received HNL and HNLS fibers; the slops of fitting lines are approximate –0.5

where Y is a geometric constant, E the modulus of elasticity (270 GPa for HNL, 420 GPa for HNLS, respectively). By substituting the fracture strength in Eq. (12) with Eq. (8), the critical fracture energies could be simplified as:

$$\gamma_c = \frac{K_{1c}^2}{2E} \tag{13}$$

The critical fracture energy calculated with Eq. (13) is 4.5 J/m^2 for as-received HNL fiber, 3.6 J/m^2 for as-received HNLS fiber, which are on the same magnitude with those of other glass materials [31]. The low critical fracture energy for HNLS fiber could be attributed to the low strain to failure (HNL: 1%, HNLS: 0.65% [11]). As for the critical fracture energies for annealed fibers, were listed in Table 1.

The Griffith theory presents a criterion for propagation of preexisting flaws that generally determines the failure of brittle materials and can be used to explain the features of fracture surface [31]. For the as-received fibers, the carbon layer covered on the surface of fibers can blunt the critical flaw and reduce the stress concentration on the surface flaw. However, this carbon layer can be removed by reaction with residual oxygen from fiber itself and atmosphere. In this case, the propagation of preexisting surface flaws will become easy. In addition, flaws produced by decomposition, active oxidation and large grain deposition can exist on the fiber's surface at high temperature resulting in the low fracture toughness. Generally, this flaw is sub-critical size. At fairly high strain rate (0.3 mm/min) at which the strengths were measured, this flaw would propagate gradually until it becomes critical because of stress concentration around the flaw.

Combining the fracture properties with microstructure characterization of SiC-based fibers, it is clear that the strength of SiC fibers is associated with the thermal decomposition of amorphous phase, grain coarsening and active oxidation. However, we still can not deny the

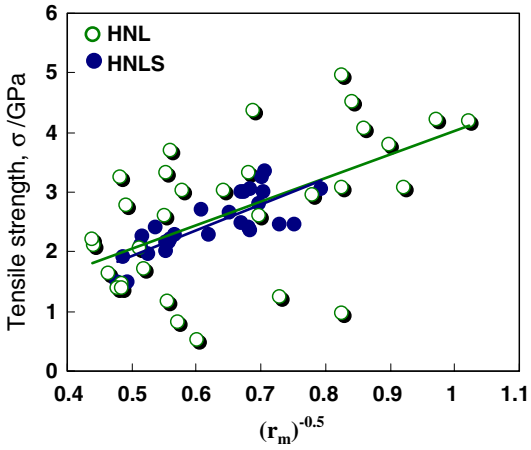

Fig. 8 The fiber tensile strength versus the square root of the fracture mirror size; the slops of fitting lines yield the mirror constant $A_m = 3.93$ MPam$^{-1/2}$ for as-received HNL fiber, $A_m = 4.33$ Mpam$^{-1/2}$ for as-received HNLS fiber

existence of other degradation mechanisms such as contaminants during annealing and metallic impurities induced during process [34–36]. The existence of metallic impurities within the fibers is possible, because all these fibers are polymer derived. The metallic impurities can easily enter the fibers during the various steps of polymer handling and can cause rapid or abnormal grain growth in local areas. There are at least two indirect observations supporting above mentioned mechanism: (i) Observation of fracture surface in Fig. 5 for the HNL and HNLS fiber showed that the strength-limiting flaws after annealing are larger than the average grain size, indicating rapid defect growth in selected areas of the fiber and thus suggesting the possible existence of metallic impurites; (ii) the UF fiber showed high strength retention than HNL fiber [23]. This suggests that the UF fiber during processing did not introduce metallic impurities to the degree that those employed for the HNL fiber.

Summary

SiC-based fibers, Hi-Nicalon™, Hi-Nicalon™ type S and Tyranno™-SA, were annealed at temperatures ranging from 1,300 to 1,900 °C in Ar for 1 h. After annealing, the microstructural characteristics and fracture properties were investigated, respectively.

As a result, excellent microstructure and mechanical stabilities were observed for SiC fibers with near-stoichiometric composition and high-crystalline structure. Also, the correlation between the mechanical properties and the microstructure of SiC-based fibers was clarified. Combining the microstructure examination with mechanical test indicates that the thermal and mechanical stabilities of SiC fibers at high temperature were mainly controlled by their crystallization and composition as well as other factors. The crystallization of amorphous phase and impurities could cause the grain coarsening, decomposition and oxidation of SiC.

Based on the present result, the near stoichiometric and high crystallite SiC fibers showed a high potential to be applied at very high temperatures. This work is useful to the optimization of fabrication and application condition of high performance CMCs.

Table 1 Fracture toughness and critical fracture energy for annealed fibers

	Condition			
	As-received	1300 °C	1400 °C	1600 °C
HNL, K_{1c}(MPa m$^{1/2}$)	1.56	1.46	1.40	1.27
HNL, γ_c (J/m^2)	4.51	3.95	3.63	2.99
HNLS, K_{1c}(MPa m$^{1/2}$)	1.74	1.61	1.45	1.34
HNLS, γ_c (J/m^2)	3.60	3.09	2.50	2.14

References

1. Kohyama A (2004) Ceramics 39:838 (in Japanese)
2. Naslain R (2004) Compos Sci Technol 64:155
3. Ohnabe H, Masaki S, Onozuka M, Miyahara K, Sasa T (1999) Compos: Part A 30:489
4. Ichikawa H (2000) Ann Chim Sci Mat 25:523
5. Ishikawa T, Kohtoku Y, Kumagawa K, Yamamura T, Nagasawa T (1998) Nature 391:773
6. Dong S, Katoh Y, Kohyama A (2003) J Am Ceram Soc 86:26
7. Lee SP, Katoh Y, Park JS, Dong S, Kohyama A, Suyama S, Yoon HK (2001) J Nucl Mater 289:30
8. Dong SM, Chollon G, Labrugere C, Lahaye M, Guette A, Bruneel JL, Couzi M, Naslain R, Jiang DL (2001) J Mater Sci 36:2371
9. Havel M, Colomban Ph (2003) J Raman Spectr 34:786
10. Havel M, Colomban Ph (2004) Compos: Part B 35:139
11. Bunsell AR, Berger MH (2000) J Euro Ceram Soc 20:2249
12. Sha JJ, Nozawa T, Park JS, Katoh Y, Kohyama A (2004) J Nucl Mater 329–333:592
13. Cullity BD (1978) Elements of X-ray diffraction, 2nd edn. Addison Wesley, Reading, MA, p 284–285
14. ASTM D3379-75 (reapproved 1989) Standard test method for tensile strength and Young's modulus for high-modulus single-filament materials
15. Youngblood GE, Lewinsohn C, Jones RH, Kohyama A (2001) J Nucl Mater 289:1
16. Shimoo T, Tsukada I, Narisawa M, Seguchi T, Okamura K (1997) J Ceram Soc Jpn 105:559
17. Chollon G, Pailler R, Naslain R, Laanami F, Monthioux M, Olry P (1997) J Mater Sci 32:327
18. Ichikawa H (2000) Ann Chim Sci Mat 25:523
19. Ichikawa H, Ishikawa T (2000) In: Kelly A, Zweben C, Chou T (eds) Silicon carbide fibers (organometallic Pyrolysis), Comprehensive composite Materials, vol 1. Elsevier Science Ltd, Oxford, England, pp 107–145
20. Takeda M, Saeki A, Sakamoto J, Imai Y, Ichikawa H (1999) Compos Sci Technol 59:787

21. Yajima S, Okamura K, Matsuzawa T, Hasegawa Y, Shishido T (1979) Nature 279:706
22. Sasaki Y, Nishina Y, Sato M, Okamura K (1987) J Mater Sci 22:443
23. Sacks MD (1999) J Eur ceram soc 19:2305
24. Eelhaes P, Carmona F (1981) Chem Phys Carbon 17:89
25. Schneider B, Guette A, Naslain R, Cataldi M, Costecalde A (1998) J Mater Sci 33:535
26. Shimoo T, et al (2002) J Mater Sci 37:4361
27. Takeda M, Sakamoto J, Imai Y, Ichikawa H (1999) Compos Sci Technol 59:813
28. Shimoo T, Okamura K, Morita T (2004) J Mater Sci 39:7031
29. Kumagawa K, Yamaoka H, Shibuya M, Yamakura T (1998) Ceram Eng Sci Proc 19:65
30. Sawyer LC, Jamieson M, Brikowski D, Haider MI, Chen RT (1987) J Am Ceram Soc 70:798
31. Mecholsky JJ, Rice RW, Freiman SW (1974) J Am Ceram Soc 57:440
32. Zhu YT, Blumenthal WR, Taylor ST, Lowe TC (1997) J Am Ceram Soc 80:1447
33. Thouless MD, Sbaizero O, Sigl LS, Evans AG (1989) J Am Ceram Soc 72:525
34. Toreki Wm, Batich CD, Sacks MD, Saleem M, Choi GJ, Morrone AA (1994) Compos Sci Technol 51:145
35. Ramberg CE, Worrell WL (2001) J Am Ceram Soc 84:2607
36. Mazdiyasni KS, Aangvil A (1985) J Am Ceram Soc 68:C-142